ARTICLE

Check for updates

Spin-triplet pairing induced by near-neighbor attraction in the extended Hubbard model for cuprate chain

Dai-Wei Qu[1,2], Bin-Bin Chen [3], Hong-Chen Jiang[4], Yao Wang [5✉] & Wei Li [2,6✉]

In quantum materials, the electronic interaction and the electron-phonon coupling are, in general, two essential ingredients, the combined impact of which may drive exotic phases. Recently, an anomalously strong electron-electron attraction, likely mediated by phonons, has been proposed in one-dimensional copper-oxide chain $Ba_{2-x}Sr_xCuO_{3+\delta}$. Yet, it is unclear how this strong near-neighbor attraction V influences the superconductivity pairing in the system. Here we perform accurate many-body calculations to study the extended Hubbard model with on-site Coulomb repulsion $U > 0$ and near-neighbor attraction $V < 0$ that could well describe the cuprate chain and likely other similar transition-metal materials with both strong correlations and lattice effects. We find a rich quantum phase diagram containing an intriguing Tomonaga-Luttinger liquid phase — besides the spin density wave and various phase separation phases — that can host dominant spin-triplet pairing correlations and divergent superconductive susceptibility. Upon doping, the spin-triplet superconducting regime can be further broadened, offering a feasible mechanism to realize p-wave superconductivity in realistic cuprate chains.

[1] Kavli Institute for Theoretical Sciences, University of Chinese Academy of Sciences, 100190 Beijing, China. [2] CAS Key Laboratory of Theoretical Physics, Institute of Theoretical Physics, Chinese Academy of Sciences, 100190 Beijing, China. [3] Department of Physics and HKU-UCAS Joint Institute of Theoretical and Computational Physics, The University of Hong Kong, Pokfulam Road, Hong Kong, China. [4] Stanford Institute for Materials and Energy Sciences, SLAC National Accelerator Laboratory and Stanford University, Menlo Park, CA 94025, USA. [5] Department of Physics and Astronomy, Clemson University, Clemson, SC 29631, USA. [6] CAS Center for Excellence in Topological Quantum Computation, University of Chinese Academy of Sciences, 100049 Beijing, China. ✉email: yaowang@g.clemson.edu; w.li@itp.ac.cn

S trongly correlated materials, where the electronic structure cannot be approximated by the reductive band theory, have become a research frontier. In particular, two types of unconventional superconductivity have attracted considerable attention. One of them is the high-T_c superconductivity discovered in cuprates[1]. Although this class of materials has been investigated for nearly 40 years, the pairing mechanism remains an enigma[2–5]. The other type of unconventional superconductivity is the topological triplet-pairing superconductivity[6–8], where electron fractionalizes into Majorana excitations[9,10] and is the foundation for topological quantum computing[11,12]. Therefore, pursuing such exotic superconductivity in realistic compounds constitutes a stimulating research topic.

The single-band Hubbard model, as the prototypical model carrying the strong correlation effects, has been widely employed in the studies of many-electron systems[13–18] as variants of this model are relevant to the two-dimensional (2D) cuprate superconductors. Besides, quasi-1D cuprate chains also constitute important class of strongly correlated materials that host intriguing correlated electron states and effects, e.g., the Tomonaga-Luttinger liquid (TLL) with spin-charge separation[19–21]. On the other hand, most theoretical studies of the ground-state and dynamical properties[22–25] also lie in 1D as rigorous many-body simulations are more accessible using analytics[26], exact diagonalization[27–30], density matrix renormalization group (DMRG)[31–34] and quantum Monte Carlo[35–41]. Since both the on-site interaction U and near-neighbor (NN) interaction V correspond to the electronic repulsion at different distances, previous numerical studies focused on the cases with repulsive $U, V > 0$ as supposed relevant to real materials[36,41–45].

Most recently, a paradigm shift occurs as an in situ ARPES experiment on the 1D cuprate chain $Ba_{2−x}Sr_xCuO_{3+\delta}$ (BSCO) suggests an anomalously strong attraction $V < 0$ between NN electrons[46]. In contrast to the intrinsic electron-electron Coulomb repulsion, this attractive interaction is likely to be mediated by electron-phonon coupling[47]. Although a rigorous identification of its origin and precise quantification of its strength may require more experimental measurements, this discovery reveals the possibility of a positive-U and negative-V system in the transition metal oxides, where strong correlations and electron-phonon coupling widely coexist[48–53]. Such an effective attraction largely missed previously may serve as a key ingredient in both understanding the high-T_c superconductivity and enabling exotic quantum phases in correlated materials[27–30,54–63]. Therefore, an interesting question naturally arises: Does such an effective attraction V help establish superconducting pairing between the strongly correlated electrons?

To address this question, and also motivated by the recent experimental realization of such attractive-V extended Hubbard model (EHM, see Fig. 1a), we employ large-scale DMRG simulations and systematically explore its phase diagram. We especially focus on the possible realization of spin-triplet superconductivity while identifying all phases. At both half and quarter fillings, we have numerically determined the ground-state phase diagrams of the EHM, from which we identify a robust gapless TLL phase with a prominent spin-triplet superconducting (TS) pairing with algebraic singularity. In two dimensions, the triplet superconducting state is topologically non-trivial where the fractional excitation can emerge on the boundary[10,64–67]. However, quantum fluctuations are usually too strong in 1D such that interacting electrons in a Hubbard-type chain usually behave as a TLL, contradicting the mean-field and small-cluster predictions. Therefore in this paper, we refer to this emergent TLL phase with divergent superconducting susceptibility as a gapless TS phase.

Our main findings are summarized in Fig. 1. At half filling (see Fig. 1b), the TS phase survives only up to a finite $U_c/t \simeq 2.3$ and is
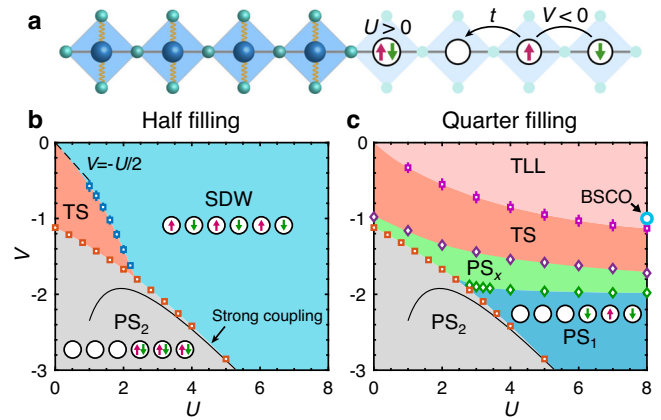
Fig. 1 Extended Hubbard model and phase diagrams. a illustrates the BSCO compound and corresponding extended t-U-V Hubbard model with NN hopping t, on-site repulsive U, and NN attractive V terms. **b, c** show the quantum phase diagrams of the EHM at half and quarter fillings, respectively. There are triplet superconducting (TS), spin density wave (SDW), and Tomonaga-Luttinger liquid (TLL) phases. There are also three phase separation phases with singly (PS_1) doubly (PS_2) or fractionally (PS_x) occupied clusters. The solid black lines represent the asymptotic phase boundary $V = -\frac{U}{2} - \frac{8\ln 2}{3U}$ in the strong coupling limit, and the dashed line for $V = -U/2$ in the weak coupling limit[30,54]. The blue circle in **c** represents the parameters $U = 8$ and $V = -1$ of the doped 1D cuprate chain BSCO[46].

absent when $U > U_c$. At quarter filling (see Fig. 1c), this TS phase extends to larger Us comparable to those in cuprates[46,68,69]. Between this TS phase and the regular phase separation (PS) phases with singly (PS_1) and doubly (PS_2) occupied clusters, we further identify an exotic PS_x phase where the clustered electrons form the TLL and even TS states. With the model parameters determined from fitting dynamical data of BSCO[46], our study reveals a close proximity of this doped cuprate chain to the p-wave superconductivity, and provide theoretical guide for realizing such gapless TS phase in 1D cuprate chains.

Results

EHM with NN attraction. We consider the minimal model for BSCO chain, i.e., EHM with on-site $U > 0$ and NN attraction $V < 0$[46], whose Hamiltonian reads

$$H = -t \sum_{i=1,\sigma}^{L-1} (c_{i\sigma}^\dagger c_{i+1\sigma} + \text{H.c.}) + U \sum_{i=1}^{L} n_{i\uparrow} n_{i\downarrow} + V \sum_{i=1}^{L-1} n_i n_{i+1}, \quad (1)$$

where $c_{i\sigma}^\dagger$ ($c_{i\sigma}$) is the electron creation (annihilation) operator, $\sigma = \uparrow, \downarrow$ labels the electron spin, and $n_i = n_{i\uparrow} + n_{i\downarrow}$ is the particle number operator at site i. Throughout the study, we set hopping amplitude $t = 1$ as the energy unit, and focus on the ground state phase diagrams at both half and quarter fillings. In this work, we employ DMRG method with non-Abelian symmetry implemented[70,71] (see "Methods" and Supplementary Note 1).

To characterize various quantum phases, we compute the spin, charge, and pairing correlation functions. The spin-spin correlation is defined as $F(r) = \langle \mathbf{S}_i \cdot \mathbf{S}_j \rangle$, with $\mathbf{S}_{i(j)}$ the spin operator at site $i(j)$ and $r \equiv j - i$. The charge density correlation is defined as $D(r) = \langle n_i n_j \rangle - \langle n_i \rangle \langle n_j \rangle$, where $n_{i(j)}$ is the particle number operator at site $i(j)$. To characterize the superconducting (SC) pairing correlation, we consider both the spin-singlet (s-wave) pairing $\Phi_S(r) = \langle \Delta_S^\dagger(i) \Delta_S(j) \rangle$ with $\Delta_S^\dagger(i) = \frac{1}{\sqrt{2}}(c_{i,\uparrow}^\dagger c_{i+1,\downarrow}^\dagger - c_{i,\downarrow}^\dagger c_{i+1,\uparrow}^\dagger)$, and the triplet ($p$-wave) pairing $\Phi_{T,s}(r) = \langle \Delta_{T,s}^\dagger(i) \Delta_{T,s}(j) \rangle$ with three components $\Delta_{T,1}^\dagger(i) = c_{i,\uparrow}^\dagger c_{i+1,\uparrow}^\dagger$, $\Delta_{T,0}^\dagger(i) = \frac{1}{\sqrt{2}}(c_{i,\uparrow}^\dagger c_{i+1,\downarrow}^\dagger + c_{i,\downarrow}^\dagger c_{i+1,\uparrow}^\dagger)$, and

$\Delta^\dagger_{T,-1}(i) = c^\dagger_{i,\downarrow} c^\dagger_{i+1,\downarrow}$ for $s = 1, 0, -1$, respectively. Note that the EHM in Eq. (1) is SU(2) invariant so the above three components are degenerate in the spin-triplet channel, and we thus take the averaged $\Phi_T(r) = \frac{1}{3}\sum_s \Phi_{T,s}(r)$ from our SU(2) DMRG calculations and compare it with Φ_S.

Analytical results from the TLL theory. The TLL theory puts rigorous constraints[72–75] on numerical results, which we always compare with and make use of in the analysis of our numerical data. In TLL, two-point correlation functions including the spin, charge and pairing correlations all decay in power law $\sim r^{-\alpha}$, with exponents α determined by two basic Luttinger parameters K_σ and K_ρ, respectively related to the spin and charge degrees of freedom (see more details in the Supplementary Note 2). To accurately evaluate these intrinsic parameters, one can calculate the momentum-dependent spin structure factor $S_m(k)$ and charge structure factor $S_c(k)$, and then extract K_σ and K_ρ.

For the current EHM in Eq. (1) with SU(2) spin symmetry, $K_\sigma = 1$ for the spin density wave (SDW), TLL, and TS phases with gapless spin excitations, while $K_\sigma = 0$ in the spin gapped phase PS$_2$. Therefore, K_ρ uniquely determines the power-law exponents α of various correlations: for charge and spin correlations there exist a uniform mode with exponent $\alpha_0 = 2$ and a $2k_F$ mode with $\alpha_{2k_F} = 1 + K_\rho$; for the pairing correlations Φ_S and Φ_T, they both have uniform modes with the same exponent $\alpha_{SC} = 1 + 1/K_\rho$, which dominates over the spin and charge correlations when $K_\rho > 1$. Consequently, the low-T behaviors of the staggered magnetic, charge, and pairing susceptibilities are also controlled by K_ρ, i.e., $\chi_{SDW} \sim T^{K_\rho-1}$, $\chi_{CDW} \sim T^{K_\rho-1}$, and $\chi_{SC} \sim T^{1/K_\rho-1}$. For $K_\rho > 1$ or <1, these susceptibilities exhibit apparently distinct behaviors as $T \to 0$. Thus, the Luttinger parameter constitutes an essential quantity characterizing the underlying phases of a 1D system. In practice, we extract the Luttinger parameter K_ρ via a second-order polynomial fitting of $S_c(k)$ in the small k regime[41,45,73,76] (see Supplementary Note 3 for details). To minimize the boundary effect, we evaluate the correlation functions using sites away from both ends.

Quantum phase diagram at half filling. We summarize our main findings at half filling in the phase diagram of Fig. 1b, where the SDW, phase separation PS$_2$ with doubly occupied sites clustered, and most remarkably, a TLL phase with prominent superconductive pairing is uncovered. To show the distinction of these phases, we present simulations along two typical paths in Fig. 2, namely, the $U = 1.6$ and $U = 4$ vertical cuts in the phase diagram.

The Luttinger parameter K_ρ clearly separates the $U = 1.6$ systems into three regimes. As the interaction strength increases to $|V| > |V_c| \simeq 1$ (but smaller than the phase separation transition strength $|V_s|$, which will be discussed later), in Fig. 2a there exists an intermediate regime with $K_\rho > 1$. We also compute the central charge c by fitting the entanglement entropy (see more details in Supplementary Note 4), and from Fig. 2b c is found to change from $c \simeq 1$ to about 2 for $|V_c| < |V| < |V_s|$, confirming that the intermediate phase has both gapless spin and charge modes. On the other hand, also as shown in Fig. 2, for the $U = 4$ case K_ρ remains small for all values of V and does not exceed 1 (see Fig. 2d) and the central charge remains $c = 1$ (Fig. 2e), showing the absence of such intermediate phase.

With further increase of the attractive interaction for either $U = 1.6$ or 4, the system eventually exhibits phase separation for $|V| > |V_s|$. The critical strength V_s dependent on U is shown in Fig. 1 (see the detailed estimation of V_s in Supplementary Note 1). Specifically for the two selected cuts, we found $V_s \simeq -1.55$ for $U = 1.6$ (see Fig. 2a–c) and $V_s \simeq -2.42$ for $U = 4$ (see Fig. 2d–f).
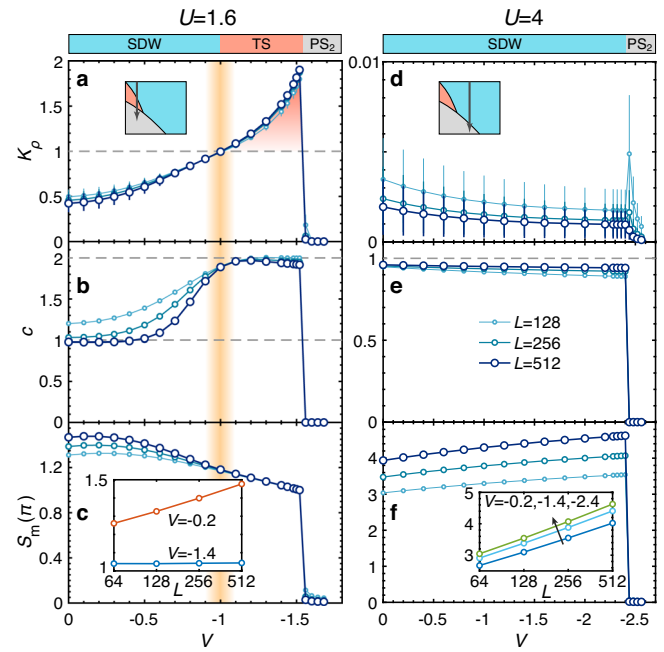
Fig. 2 Results of EHM at half filling. a–c are with on-site repulsion of $U = 1.6$ and **d–f** of $U = 4$, with the corresponding mini phase diagrams also depicted. **a, d** show the results of the Luttinger parameter K_ρ, (**b, e**) are the results of central charge c determined from the entanglement entropy scalings, and **c, f** are the spin structure factors at π. Here the K_ρ results in **a, d** are obtained via the second-order polynomial fitting of $S_c(k)$ in the small-k regime, with the error bars estimated by using different k-range for fitting (Supplementary Note 3). The insets in **c, f** show $S_m(\pi)$ vs. L at various Vs. **a–c** reveal the system undergoes a transition from spin density wave (SDW) to triplet superconducting (TS) phase at $V_c \simeq -1$ and then enters the phase separation (PS$_2$) regime for $V < V_s \simeq -1.55$. **d–f** show no intermediate phase but a direct first-order transition from SDW to PS$_2$ at $V_s \simeq -2.42$.

In such a PS state, the clustered part consists of doubly-occupied sites and no singularity can be observed in various correlations. Therefore, we denote it as PS$_2$ to distinguish from other PS phases discussed later.

Among these three phases in the $U = 1.6$ case (and for other interactions $U < U_c \simeq 2.3$, c.f., Fig. 1b), we are particularly interested in the intermediate one due to the signature of triplet pairing. As evidenced by the charge correlation results in Fig. 3a, the charge gap is closed by the attractive V term, and the Luttinger parameter K_ρ can be fitted to be greater than 1 (see the inset of Fig. 3a, and more details in Supplementary Note 3). According to the TLL theory, the superconductive paring decays $r^{-\alpha_{SC}}$ with the exponent $\alpha_{SC} = 1 + 1/K_\rho$— smaller than the algebraic exponent $(1 + K_\rho)$ of both the charge and spin correlations when $K_\rho > 1$— and thus constitutes the dominant correlation in the charge-2e channel, with an algebraically diverging pairing susceptibility $\chi_{SC}(T)$ for low temperature T.

In the weak attraction regime $|V| < |V_c|$, K_ρ remains finite (< 1) in Fig. 2a due to the strong finite-size effects and a small charge gap for $U = 1.6$, which would converge to zero in the thermodynamic limit. $K_\sigma = 1$ due to the spin SU(2) symmetry. In Fig. 3b, an quasi-long range spin order with an algebraic exponent of $\alpha_{SDW} = 1$ appears, which has logarithmically diverging spin structure factor of $S_m(k = \pi)$ (see Fig. 2c, f and the insets). This is well consistent with the SDW scenario with a finite charge gap and quasi-long range spin order (see Supplementary Note 5). On the other hand, for the intermediate

3
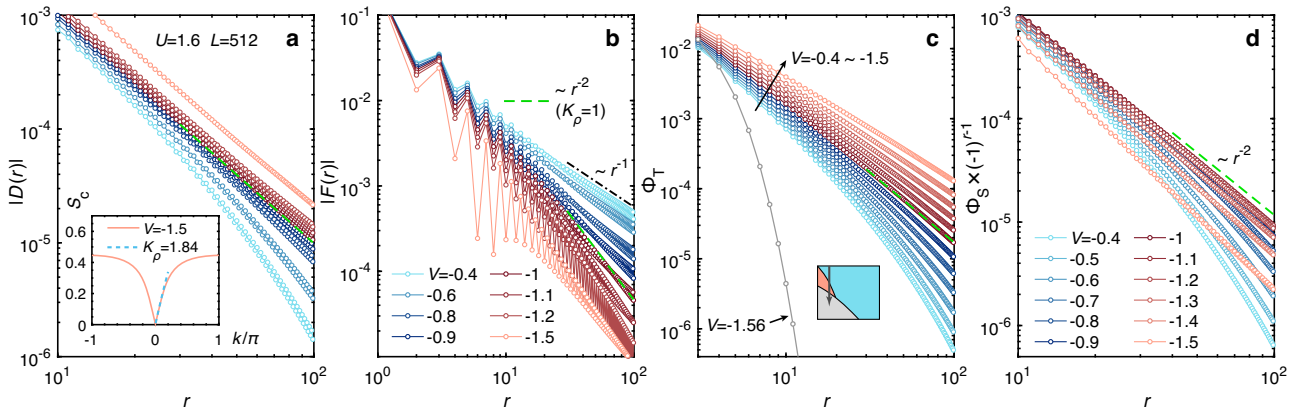
Fig. 3 Correlation functions of the half-filled EHM at $U = 1.6$. Here we show **a** density-density, **b** spin-spin, **c** the spin-triplet pairing, and **d** singlet pairing correlations, with various attractive interactions $-1.5 \leq V \leq -0.4$. The color codes in the four panels are the same (following the representative color of each phase in Fig. 1b, as indicated by the legends in **b**, **d**). The dashed green line represents $\sim r^{-2}$ scaling that corresponds to $K_\rho = 1$, separating the exponential and power-law behaviors of various correlations in **a**, **c**, **d**. The dotted dash line $\sim r^{-1}$ with exponent $\alpha = 1$ in **b** represents long-distance scaling of the spin correlations in the SDW phase. The inset in **a** shows the charge structure factor at $V = -1.5$, whose second-order polynomial fitting (dashed cyan line) results in a Luttinger parameter of $K_\rho = 1.84$.
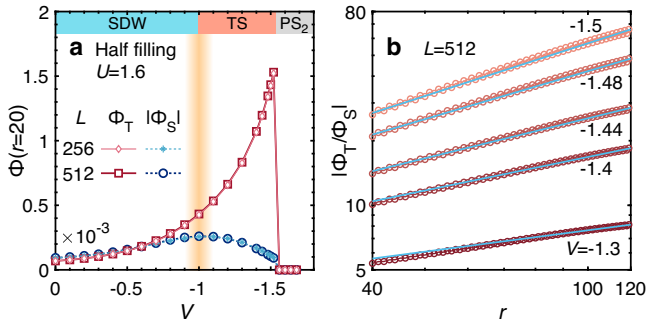
Fig. 4 Dominance of the triplet over singlet pairing in the half-filled TS phase. Here we show the data of $U = 1.6$. **a** Singlet and triplet pairing correlations at a fixed (long) distance $r = 20$. The yellow strip represents the transition point $V_c \simeq -1$ from spin density wave (SDW) to triplet superconducting (TS) phase. **b** The calculated ratios $|\Phi_T / \Phi_S|$, plotted in a log-log scale, exhibit excellent agreement with the scaling $r^{K_\rho - 1}$ (blue solid lines).

phase in Fig. 2c $S_m(\pi)$ ceases to increase vs. L, as the $2k_F$ mode spin correlation decays faster than $\sim r^{-2}$ shown in Fig. 3b, which reveals a non-diverging magnetic susceptibility and thus rather distinct magnetic properties from that of the SDW phase.

Gapless triplet superconducting phase. As shown in Fig. 3c, d, it can be observed that both the singlet- (Φ_S) and triplet-pairing (Φ_T) exhibit power-law decay behaviors, and the latter with p-wave pairing symmetry clearly dominates over the former with the s-wave pairing symmetry. This is clearly demonstrated in Fig. 4a, where the strengths of the two correlations $\Phi_T(r)$ and $\Phi_S(r)$ are compared at a fixed distance $r = 20$. Though two pairing correlations are comparable in the SDW regime, $\Phi_T(r)$ clearly surpasses $\Phi_S(r)$ once entering the intermediate-V phase: the latter turns to decreasing, while $\Phi_T(r)$ keeps increasing and becomes over one order of magnitude greater than $\Phi_S(r)$.

Such a dominance of the triplet pairing in the TS phase holds for different distances r other than the fixed distance $r = 20$ in Fig. 4a. This dominance is reflected in the spatial distribution of both pairing correlations in Fig. 3c, d. There we find Φ_T firstly decays exponentially in the SDW phase (the blue dots), then exhibits power-law behaviors for $|V_c| < |V| < |V_s|$ (the red dots),

and decays again exponentially for $|V| > |V_s|$ (the gray dots). We notice there is virtually no uniform but only $2k_F$ mode in Φ_S, as reflected in the smooth curves $\Phi_S(r) \times (-1)^{r-1}$ in Fig. 3d. For the gapless TS phase where we are most interested in, the dominance of Φ_T is reflected by the comparison of Fig. 3c and d: $\Phi_T(r)$ decays slower than r^{-2}, while $\Phi_S(r)$ decays faster than r^{-2} (Fig. 3d). More quantitatively, the ratio between these two pairing correlations $|\Phi_T(r)/\Phi_S(r)|$ scales in power law $r^{K_\rho - 1}$, since the leading scaling in Φ_T and Φ_S is $1/r^{1+1/K_\rho}$ and $1/r^{K_\rho + 1/K_\rho}$, respectively (see Supplementary Note 2). We present such a power-law scaling extracted from our DMRG simulations in Fig 4b. Therefore, in the intermediate regime the pairing correlation Φ_T dominates over Φ_S not only in magnitude but actually in long-distance scaling, making it a rather unique gapless TS phase.

When compared to the phase diagram obtained in ref. [54], our DMRG results in Fig. 1b show some agreement on the existence of three phases, yet there are still noticeable differences. Particularly, our DMRG calculations identify the upper boundary of the TS phase in agreement with $V = -U/2$ obtained from the perturbation theory in the small U regime while it deviates from this line in the strong coupling regime. Consequently, in contrary to ref. [54] where the TS phase was shown extending to infinite U, our results in Fig. 1b suggest it can only survive up to $U_c \simeq 2.3$, located in a much narrower regime. On the other hand, when compared to more recent studies [62,77] where the phase diagrams are only schematic, here we pinpoint the numerically accurate phase boundaries with large-scale DMRG calculations and reveal the predominant triplet quasi-long range TS pairing relevant to the realistic cuprate chain BSCO, decades after such a TS instability was proposed [29,54].

Finite doping. Besides half filling, we have also explored the phases in the doped EHM systems. We first focus on the quarter filling, where the triplet pairing instability is approximately maximized, as will be discussed later. The extracted phase diagram is presented in Fig. 1c. Here, we select a cut along $U = 4$ and explain the properties of each phase in Fig. 5. Similar to half filling, the Luttinger parameter $K_\rho > 1$ characterizes the intrinsic nature of the correlations and separates the $U = 4$ systems into four phases (see Fig. 5a). Particularly, for $V < V_c \simeq -0.8$, we identified a TS regime following the same principle as half filling, manifested as enhanced triplet and singlet pairing correlations.
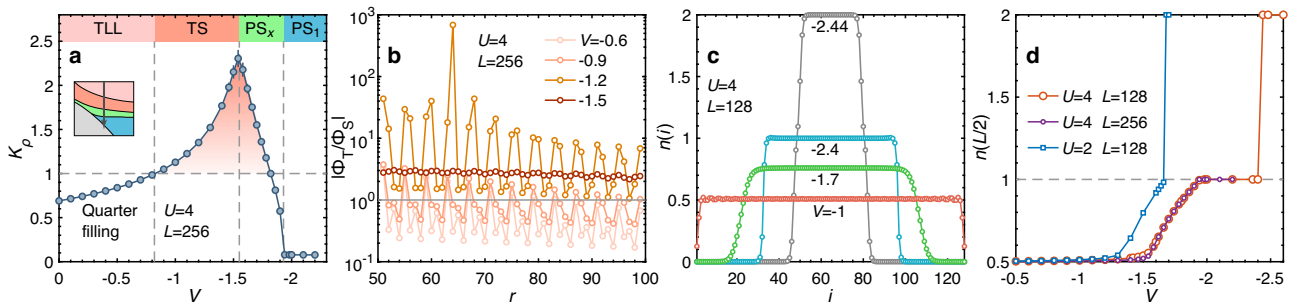
Fig. 5 Results of EHM at quarter filling. We show in **a** the mini phase diagram and Luttinger parameter K_ρ, and **b** accordingly the ratio between triplet and singlet pairings $|\Phi_T/\Phi_S|$ that becomes greater than 1 in the emergent TS phase. The K_ρ results in the PS_x and PS_1 are computed within the clustered part (see Supplementary Note 3). **c** The charge distribution $n(i)$ in TS ($V = -1$), PS_x ($V = -1.7$), PS_1 ($V = -2.4$), and PS_2 ($V = -2.44$) phases, respectively. **d** The charge densities $n(L/2)$ measured at the center of the system are plotted versus V.

Between these two correlations, we evaluated their ratio $|\Phi_T/\Phi_S|$ and found its envelop increasing monotonically as $|V|$ enhances and exceeding 1 for $V < V_c$ (see Fig. 5b), despite some oscillations with distance r. Note the two pairing correlations now show the same scaling at long distance. Importantly, the TS phase at quarter filling is significantly wider than that at half filling, particularly in the large U regime.

Besides the TS regime, there are three different inhomogeneous PS phases, i.e., PS_1, PS_x, and PS_2 in Fig. 1c, in the doped system. The real-space charge distributions $n(i)$ are shown in Fig. 5c, from which we see that in the PS phases the electrons cluster with filling $n = 1, 2$ or $x \in (1/2, 1]$. To track the evolution among these PS phases when V changes, we pick the center of the system as a representative, which always lies in the filled domain in a PS state due to the open boundary, and extract $n(i = L/2)$ for different U and V strengths in Fig. 5d. This filling density starts with $n(L/2) = 0.5$ (i.e., the TLL and TS phases) and deviates from the uniform quarter filling when $|V|$ is stronger than certain transition value. As $n(L/2) = x$ is not a fixed integer value but varies between 0.5 and 1, we denote this regime as PS_x. For small U, like $U = 2$, the system jumps from PS_x to PS_2 at a second transition point. In contrast, this transition is preceded by a third PS phase for large $U > U_c \simeq 2.3$ (the same as that of half filling). Taking $U = 4$ as an example, PS_x firstly transits into an $n(L/2) = 1$ phase (denoted as PS_1), and then jumps into PS_2 as $|V|$ further increases. For the doped cases with filling factors other than 1/4, the quantum phase diagram is qualitatively similar to that of Fig. 1c. The phase boundaries of PS_1 and PS_2 actually remain intact for other doping since they reflect the local energy relation between singly and doubly occupied states. The quantum many-body states in the clustered part of the three PS phases — PS_1, PS_2, and PS_x — only depends on the interaction parameters U and V.

The existence of the PS_x phase was missed in early studies on the same model[29,54], and the distinct feature of PS_x is the clustered electrons that constitute a TLL liquid with fractional filling. With x continuous tuned by V, the clustered part of PS_x can also become close to half filling in terms of density, i.e., $x = 1$. Nevertheless, it is distinct from that in the PS_1 phase, as the clustered electrons in the latter form a charge gapped SDW instead of a gapless TLL. Even more interestingly, we can also identify a $K_\rho > 1$ regime with significant TS pairing correlations in the clustered part of PS_x, showing the existence of gapless TS cluster in (at least part of) the PS_x phase (see more details in Supplementary Note 6).

Discussion

Our simulation is motivated by but not restricted to the recently extracted attractive-V extended Hubbard model for 1D cuprate

BSCO from experiments[46]. Previously, there were weak-coupling renormalization group (RG) and functional RG studies of the half-filled EHM that suggested the presence of TS pairing based on the field-theoretical analysis[54,55,61,63]. Besides, there were also ED and DMRG calculations of the phase diagram for half-filled or doped cases[28–30,56,57,59,60,62]. The TS phase is characterized by dominant triplet superconducting pairing correlation, whose long-distance scaling analysis, however, was missing in previous studies.

In this work, we employ DMRG—the method of choice for 1D correlated systems—to investigate the EHM with both on-site repulsive and near-neighbor attractive interactions. At both half and quarter fillings, we identify a prominent gapless TS phase with the p-wave pairing induced by the attractive interactions. Different from the long-range order (hidden) assumption in the context of mean-field theory, the p-wave superconducting order identified in this correlated 1D chain is quasi-long-ranged: the triplet pairing correlation Φ_T decays as a power-law at long distance and presents as the dominant charge-2e excitations in the gapless TLL, and specially, at half filling it dominates over the singlet pairing Φ_S also in large distance scaling. Such dominance results in divergent triplet superconductive susceptibility at low temperature. This phenomenon can be detected by the spectral depletion in ARPES or the Drude peak in optical conductivity, both of which are accessible for in situ synthesized quasi-1D materials.

Besides the qualitative identification of various phases, our work also pushed the exact phase diagram to a quantitative level. This is important because the interest in the 1D EHM (with $V < 0$ and $U > 0$) is no longer restricted to theoretical discussions. It has been proposed as the underlying model for 1D cuprate chains[46,47]. Therefore, a quantitatively accurate phase diagram, especially with doping dependence, will be essential for upcoming experimental investigations of the TS phase in the 1D cuprate BSCO. For example, it is noted that the phase boundaries in Fig. 1, i.e., the critical strengths of V for entering the TS phase, are U dependent, and they can be determined analytically at quarter filling in the $U \to \infty$ limit[78,79]. In this limit, the Luttinger parameter $K_\rho = 1/[2 + (4/\pi)\arcsin(v)]$ with $v = V/2$, which exceeds 1 when $|V| \geq \sqrt{2}$. According to ref. [46] the effective model parameters for 1D cuprate chain BSCO were proposed as $U \simeq 8$ and $V \simeq -1$, where the effective attraction V is still slightly below this threshold.

To search for TS in larger parameter space, we further explore the full doping dependence. To approximate the realistic materials, we fix $U = 8$ and three different values of V, and evaluate the Luttinger parameter K_ρ for a wide range of doping. As shown in Fig. 6, the uniform TS phase characterized as $K_\rho > 1$ can be realized only if $|V| > 1.2$ (and $|V| \lesssim 1.7$ before PS_x sets in), in order to
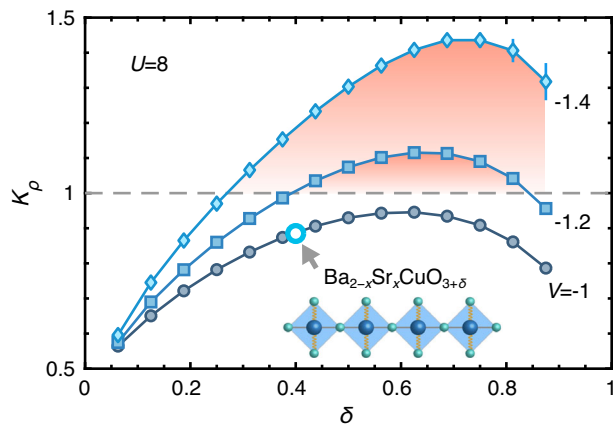
Fig. 6 Prediction for possible triplet superconducting phase in 1D cuprate chain. We show the Luttinger parameter K_ρ versus doping δ for different attractive interactions V. In the highlighted regimes with $K_\rho > 1$, there exists superconductivity phase for sufficiently strong attraction V and large doping δ. The blue circle represents the cuprate $Ba_{2-x}Sr_xCuO_{3+\delta}$ with the parameters $V = -1$[46] and $\delta \simeq 40\%$, and a slight enhancement of the attraction can drive the compound to the triplet superconductive phase.

exhibit prominent superconducting instability below 40% doping, the maximal accessible doping at current experimental conditions. Therefore, the doped BSCO resides on the boundary to a TS phase (as also indicated in Fig. 1c), and a slight reduction of on-site U or enhancement of near-neighbor attraction V may drive it into the TS phase—both can be achieved by manipulating the electron-phonon coupling either inside the crystal or via a substrate[47].

Moreover, the minimal EHM model proposed in ref. [46] can well explain the experimental observations in the BSCO chain, yet the obtained parameters can still have ~20–30% error bars, i.e., the U and V may extend a range. Recently, a numerical study actually suggests a smaller $U = 5.0t$ in BSCO chain[69], which places the compound in the TS phase according to our phase diagram (Fig. 1b) at quarter filling.

Given that, the TS phase identified in our simulations may motivate further investigation and manipulation of cuprates towards a p-wave topological superconductor. The couplings between the cuprate chains may open a charge gap and introduce edge modes that can be very useful in future quantum technologies. Due to the chemical and structural similarity between 1D and 2D cuprates, our results of the TS phase in the attractive EHM here shed light on and call for further many-body studies of the superconductivity in the EHM of higher dimensions[80–83].

Lastly, our conclusion is not restricted to the cuprate BSCO. Considering the widely existing electron repulsion and electron-phonon coupling[48–53], this model with a repulsive U and an attractive V may also be applicable, as a low-energy approximation, for other transition-metal oxides. These different cuprate compounds and other materials may exhibit different microscopic parameters (U and V) due to their distinct chemical environments, and the rich quantum phases revealed in the EHM model studies here may find their interesting materialization in these systems.

Methods

Density matrix renormalization group. We perform DMRG calculations with the charge U(1) and spin SU(2) symmetries implemented through the tensor library QSpace[70,71], and compute system sizes up to $L = 512$ to obtain the spin, charge, and superconductive correlations, etc, with high precision. In the calculations, we retain up to $m^* = 2048$ multiplets, equivalent to $m \approx 5000$ U(1) states, which render

small truncation errors $\epsilon \lesssim 10^{-7}$. We use the open boundary conditions as in conventional DMRG calculations. Due to the existence of attraction V, particularly near the PS phase one needs to introduce pinning fields at both ends and perform sufficient numbers of sweeps (even over 100 times) to fully converge the results, e.g., the charge distribution along the chain (see Supplementary Note 1).

Data availability

The data that support the findings of this study are available from the corresponding author upon reasonable request.

Code availability

All numerical codes in this paper are available upon request to the authors.

References

1. Bednorz, J. G. & Müller, K. A. Possible high T_c superconductivity in the Ba-La-Cu-O system. *Z. für. Phys. B Condens. Matter* **64**, 189–193 (1986).
2. Lee, P. A., Nagaosa, N. & Wen, X.-G. Doping a Mott insulator: Physics of high-temperature superconductivity. *Rev. Mod. Phys.* **78**, 17–85 (2006).
3. Keimer, B., Kivelson, S. A., Norman, M. R., Uchida, S. & Zaanen, J. From quantum matter to high-temperature superconductivity in copper oxides. *Nature* **518**, 179–186 (2015).
4. Proust, C. & Taillefer, L. The remarkable underlying ground states of cuprate superconductors. *Annu. Rev. Condens. Matter Phys.* **10**, 409–429 (2019).
5. Zhou, X. et al. High-temperature superconductivity. *Nat. Rev. Phys.* **3**, 462–465 (2021).
6. Sato, M. & Ando, Y. Topological superconductors: a review. *Rep. Prog. Phys.* **80**, 076501 (2017).
7. Qi, X.-L. & Zhang, S.-C. Topological insulators and superconductors. *Rev. Mod. Phys.* **83**, 1057–1110 (2011).
8. Hasan, M. Z. & Kane, C. L. Colloquium: Topological insulators. *Rev. Mod. Phys.* **82**, 3045–3067 (2010).
9. Kitaev, A. Y. Unpaired Majorana fermions in quantum wires. *Phys. -Usp.* **44**, 131–136 (2001).
10. Read, N. & Green, D. Paired states of fermions in two dimensions with breaking of parity and time-reversal symmetries and the fractional quantum Hall effect. *Phys. Rev. B* **61**, 10267 (2000).
11. Stern, A. & Lindner, N. H. Topological quantum computation-from basic concepts to first experiments. *Science* **339**, 1179–1184 (2013).
12. Nayak, C., Simon, S. H., Stern, A., Freedman, M. & Das Sarma, S. Non-Abelian anyons and topological quantum computation. *Rev. Mod. Phys.* **80**, 1083–1159 (2008).
13. Wietek, A., He, Y.-Y., White, S. R., Georges, A. & Stoudenmire, E. M. Stripes, antiferromagnetism, and the pseudogap in the doped Hubbard model at finite temperature. *Phys. Rev. X* **11**, 031007 (2021).
14. Qin, M. et al. Absence of superconductivity in the pure two-dimensional Hubbard model. *Phys. Rev. X* **10**, 031016 (2020).
15. Jiang, Y.-F., Zaanen, J., Devereaux, T. P. & Jiang, H.-C. Ground state phase diagram of the doped Hubbard model on the four-leg cylinder. *Phys. Rev. Res.* **2**, 033073 (2020).
16. Jiang, H. C. & Devereaux, T. P. Superconductivity in the doped Hubbard model and its interplay with next-nearest hopping t'. *Science* **365**, 1424–1428 (2019).
17. Zheng, B.-X. et al. Stripe order in the underdoped region of the two-dimensional Hubbard model. *Science* **358**, 1155–1160 (2017).
18. LeBlanc, J. P. F. et al. Solutions of the two-dimensional Hubbard model: Benchmarks and results from a wide range of numerical algorithms. *Phys. Rev. X* **5**, 041041 (2015).
19. Kim, C. et al. Observation of spin-charge separation in one-dimensional $SrCuO_2$. *Phys. Rev. Lett.* **77**, 4054–4057 (1996).
20. Fujisawa, H. et al. Angle-resolved photoemission study of Sr_2CuO_3. *Phys. Rev. B* **59**, 7358–7361 (1999).
21. Kim, B. J. et al. Distinct spinon and holon dispersions in photoemission spectral functions from one-dimensional $SrCuO_2$. *Nat. Phys.* **2**, 397–401 (2006).
22. Tomita, N. & Nasu, K. Quantum fluctuation effects on light absorption spectra of the one-dimensional extended Hubbard model. *Phys. Rev. B* **63**, 085107 (2001).

23. Benthien, H. & Jeckelmann, E. Spin and charge dynamics of the one-dimensional extended Hubbard model. *Phys. Rev. B* **75**, 205128 (2007).

24. Hofmann, F. & Potthoff, M. Doublon dynamics in the extended Fermi-Hubbard model. *Phys. Rev. B* **85**, 205127 (2012).

25. Al-Hassanieh, K. A., Rincón, J., Dagotto, E. & Alvarez, G. Wave-packet dynamics in the one-dimensional extended Hubbard model. *Phys. Rev. B* **88**, 045107 (2013).

26. Essler, F. H. L., Frahm, H., Göhmann, F., Klümper, A. & Korepin, V. E.The One-Dimensional Hubbard Model (Cambridge University Press, 2005).

27. Mila, F. & Zotos, X. Phase diagram of the one-dimensional extended Hubbard model at quarter-filling. *EPL (Europhys. Lett.)* **24**, 133 (1993).

28. Penc, K. & Mila, F. Phase diagram of the one-dimensional extended Hubbard model with attractive and/or repulsive interactions at quarter filling. *Phys. Rev. B* **49**, 9670–9678 (1994).

29. Lin, H. Q., Gagliano, E. & Campbell, D. K. Phase separation in the 1-D extended Hubbard model. *Phys. C. Superconductivity* **282**, 1875–1876 (1997).

30. Nakamura, M. Tricritical behavior in the extended Hubbard chains. *Phys. Rev. B* **61**, 16377–16392 (2000).

31. White, S. R. Density matrix formulation for quantum renormalization groups. *Phys. Rev. Lett.* **69**, 2863–2866 (1992).

32. Jeckelmann, E. Dynamical density-matrix renormalization-group method. *Phys. Rev. B* **66**, 045114 (2002).

33. White, S. R. & Feiguin, A. E. Real-time evolution using the density matrix renormalization group. *Phys. Rev. Lett.* **93**, 076401 (2004).

34. Benthien, H., Gebhard, F. & Jeckelmann, E. Spectral function of the one-dimensional Hubbard model away from half filling. *Phys. Rev. Lett.* **92**, 256401 (2004).

35. Hirsch, J. E. & Scalapino, D. J. $2p_F$ and $4p_F$ instabilities in a one-quarter-filled-band Hubbard model. *Phys. Rev. B* **27**, 7169–7185 (1983).

36. Hirsch, J. E. Charge-density-wave to spin-density-wave transition in the extended Hubbard model. *Phys. Rev. Lett.* **53**, 2327–2330 (1984).

37. Hirsch, J. E. & Scalapino, D. J. $2p_F$ and $4p_F$ instabilities in the one-dimensional Hubbard model. *Phys. Rev. B* **29**, 5554–5561 (1984).

38. Preuss, R. et al. Spectral properties of the one-dimensional Hubbard model. *Phys. Rev. Lett.* **73**, 732–735 (1994).

39. Rigol, M., Muramatsu, A., Batrouni, G. G. & Scalettar, R. T. Local quantum criticality in confined fermions on optical lattices. *Phys. Rev. Lett.* **91**, 130403 (2003).

40. Lavalle, C., Arikawa, M., Capponi, S., Assaad, F. F. & Muramatsu, A. Antiholons in one-dimensional $t−J$ models. *Phys. Rev. Lett.* **90**, 216401 (2003).

41. Sandvik, A. W., Balents, L. & Campbell, D. K. Ground state phases of the half-filled one-dimensional extended Hubbard model. *Phys. Rev. Lett.* **92**, 236401 (2004).

42. Tsuchiizu, M. & Furusaki, A. Phase diagram of the one-dimensional extended Hubbard model at half filling. *Phys. Rev. Lett.* **88**, 056402 (2002).

43. Jeckelmann, E. Ground-state phase diagram of a half-filled one-dimensional extended Hubbard model. *Phys. Rev. Lett.* **89**, 236401 (2002).

44. Zhang, Y. Z. Dimerization in a half-filled one-dimensional extended Hubbard model. *Phys. Rev. Lett.* **92**, 246404 (2004).

45. Ejima, S. & Nishimoto, S. Phase diagram of the one-dimensional half-filled extended Hubbard model. *Phys. Rev. Lett.* **99**, 216403 (2007).

46. Chen, Z. et al. Anomalously strong near-neighbor attraction in doped 1D cuprate chains. *Science* **373**, 1235–1239 (2021).

47. Wang, Y. et al. Phonon-mediated long-range attractive interaction in one-dimensional cuprates. *Phys. Rev. Lett.* **127**, 197003 (2021).

48. Pintschovius, L. et al. Phonon anomalies in La$_2$NiO$_4$. *EPL (Europhys. Lett.)* **5**, 247 (1988).

49. Tranquada, J. M., Buttrey, D., Sachan, V. & Lorenzo, J. Simultaneous ordering of holes and spins in La$_2$NiO$_{4.125}$. *Phys. Rev. Lett.* **73**, 1003 (1994).

50. Ramirez, A. et al. Thermodynamic and electron diffraction signatures of charge and spin ordering in La$_{1−x}$Ca$_x$MnO$_3$. *Phys. Rev. Lett.* **76**, 3188 (1996).

51. Kim, B. et al. Phase-sensitive observation of a spin-orbital Mott state in Sr$_2$IrO$_4$. *Science* **323**, 1329–1332 (2009).

52. Edwards, D. Ferromagnetism and electron-phonon coupling in the manganites. *Adv. Phys.* **51**, 1259–1318 (2002).

53. Hu, Y. et al. Spectroscopic evidence for electron-boson coupling in electron-doped Sr$_2$IrO$_4$. *Phys. Rev. Lett.* **123**, 216402 (2019).

54. Lin, H. Q. & Hirsch, J. E. Condensation transition in the one-dimensional extended Hubbard model. *Phys. Rev. B* **33**, 8155–8163 (1986).

55. Voit, J. Phase diagram and correlation functions of the half-filled extended Hubbard model in one dimension. *Phys. Rev. B* **45**, 4027–4042 (1992).

56. Kuroki, K., Kusakabe, K. & Aoki, H. Phase diagram of the extended attractive Hubbard model in one dimension. *Phys. Rev. B* **50**, 575–578 (1994).

57. Sano, K. & Ōno, Y. Electronic structure of one-dimensional extended Hubbard model. *J. Phys. Soc. Jpn.* **63**, 1250–1253 (1994).

58. Lin, H., Gagliano, E., Campbell, D., Fradkin, E. & Gubernatis, J.The phase diagram of the one-dimensional extended Hubbard model. In *The Hubbard Model*, 315-326 (Springer, 1995). https://doi.org/10.1007/978-1-4899-1042-4_35.

59. Lin, H. Q., Campbell, D. K. & Clay, R. T. Broken symmetries in the one-dimensional extended Hubbard model. *Chin. J. Phys.* **38**, 1 (2000).

60. Gu, S.-J., Deng, S.-S., Li, Y.-Q. & Lin, H.-Q. Entanglement and quantum phase transition in the extended Hubbard model. *Phys. Rev. Lett.* **93**, 086402 (2004).

61. Ménard, M. & Bourbonnais, C. Renormalization group analysis of the one-dimensional extended Hubbard model. *Phys. Rev. B* **83**, 075111 (2011).

62. Iemini, F., Maciel, T. O. & Vianna, R. O. Entanglement of indistinguishable particles as a probe for quantum phase transitions in the extended Hubbard model. *Phys. Rev. B* **92**, 075423 (2015).

63. Xiang, Y.-Y., Liu, X.-J., Yuan, Y.-H., Cao, J. & Tang, C.-M. Doping dependence of the phase diagram in one-dimensional extended Hubbard model: a functional renormalization group study. *J. Phys.: Condens. Matter* **31**, 125601 (2019).

64. Sarma, S. D., Nayak, C. & Tewari, S. Proposal to stabilize and detect half-quantum vortices in strontium ruthenate thin films: Non-Abelian braiding statistics of vortices in a $p_x + ip_y$ superconductor. *Phys. Rev. B* **73**, 220502 (2006).

65. Bolech, C. & Demler, E. Observing Majorana bound states in p-wave superconductors using noise measurements in tunneling experiments. *Phys. Rev. Lett.* **98**, 237002 (2007).

66. Tewari, S., Sarma, S. D. & Lee, D.-H. Index theorem for the zero modes of Majorana fermion vortices in chiral p-wave superconductors. *Phys. Rev. Lett.* **99**, 037001 (2007).

67. Sau, J. D., Lutchyn, R. M., Tewari, S. & Sarma, S. D. Robustness of Majorana fermions in proximity-induced superconductors. *Phys. Rev. B* **82**, 094522 (2010).

68. Jin, H.-S., Pickett, W. E. & Lee, K.-W. Two-band conduction and nesting instabilities in superconducting Ba$_2$CuO$_{3+\delta}$: First-principles study. *Phys. Rev. B* **104**, 054516 (2021).

69. Li, S., Nocera, A., Kumar, U. & Johnston, S. Particle-hole asymmetry in the dynamical spin and charge responses of corner-shared 1D cuprates. *Commun. Phys.* **4**, 217 (2021).

70. Weichselbaum, A. Non-Abelian symmetries in tensor networks : A quantum symmetry space approach. *Ann. Phys.* **327**, 2972–3047 (2012).

71. Weichselbaum, A. X-symbols for non-Abelian symmetries in tensor networks. *Phys. Rev. Res.* **2**, 023385 (2020).

72. Haldane, F. D. M. General relation of correlation exponents and spectral properties of one-dimensional Fermi systems: Application to the anisotropic $S = \frac{1}{2}$ Heisenberg chain. *Phys. Rev. Lett.* **45**, 1358–1362 (1980).

73. T., Giamarchi. Quantum Physics in One Dimension (Clarendon Press, 2004).

74. Fradkin, E.Field Theories of Condensed Matter Physics (Cambridge University Press, 2013).

75. Voit, J. One-dimensional Fermi liquids. *Rep. Prog. Phys.* **58**, 977–1116 (1995).

76. Moreno, A., Muramatsu, A. & Manmana, S. R. Ground-state phase diagram of the one-dimensional t-J model. *Phys. Rev. B* **83**, 205113 (2011).

77. Mendoza-Arenas, J. J. Dynamical quantum phase transitions in the one-dimensional extended Fermi-Hubbard model. *J. Stat. Mech.* **2022**, 043101 (2022).

78. Luther, A. & Peschel, I. Calculation of critical exponents in two dimensions from quantum field theory in one dimension. *Phys. Rev. B* **12**, 3908–3917 (1975).

79. Schulz, H. J. Correlation exponents and the metal-insulator transition in the one-dimensional Hubbard model. *Phys. Rev. Lett.* **64**, 2831–2834 (1990).

80. Sénéchal, D., Day, A. G. R., Bouliane, V. & Tremblay, A.-M. S. Resilience of d-wave superconductivity to nearest-neighbor repulsion. *Phys. Rev. B* **87**, 075123 (2013).

81. Plonka, N., Jia, C. J., Wang, Y., Moritz, B. & Devereaux, T. P. Fidelity study of superconductivity in extended Hubbard models. *Phys. Rev. B* **92**, 024503 (2015).

82. Paki, J., Terletska, H., Iskakov, S. & Gull, E. Charge order and antiferromagnetism in the extended Hubbard model. *Phys. Rev. B* **99**, 245146 (2019).

83. Jiang, M. Enhancing d-wave superconductivity with nearest-neighbor attraction in the extended Hubbard model. *Phys. Rev. B* **105**, 024510 (2022).

Acknowledgements

Author contributions

W.L. and Y.W. initiated this work. D.W.Q and B.B.C performed the DMRG calculations. All authors contributed to the analysis of the results. W.L., Y.W., and H.C.J. supervised the project.

Competing interests

The authors declare no competing interests.

Additional information

Supplementary information The online version contains supplementary material available at https://doi.org/10.1038/s42005-022-01030-x.

Correspondence and requests for materials should be addressed to Yao Wang or Wei Li.

Peer review information *Communications Physics* thanks the anonymous reviewers for their contribution to the peer review of this work. Peer reviewer reports are available.

Reprints and permission information is available at http://www.nature.com/reprints